

Influence of Ni and S co-doping of SnO₂ on Its Electrochemical Performance

Minmin Guo^{1,*}, Huimin Yang², Yuting Du¹, Jianfeng Fan¹

¹ Department of Chemistry, Xinzhou Teachers University, Xinzhou 034000, PR China

² College of Chemistry and Chemical Engineering, Taiyuan University of Technology, Taiyuan 030024, PR China

*E-mail: minminguo0804@sina.com

Received: 13 October 2020 / Accepted: 16 December 2020 / Published: 31 January 2021

SnO₂ has received considerable interest in the electrochemical field due to its low cost, good stability and easy fabrication. However, the drawback of low electrocatalytic efficiency remains great challenge to overcome. Thus, the (Ni, S) co-doped SnO₂, Ni doped SnO₂, S doped SnO₂ and pure SnO₂ nanoparticles were prepared by hydrothermal method to address this problem. The surface morphology, crystal configuration and valence state of element of the samples were characterised. The cyclic voltammetry curve, linear sweep voltammetry and electrochemical impedance curve were determined using a three-electrode system. Meanwhile, the electronic structure of the samples was investigated by first principle calculation. Compared with SnO₂, the sample has a more uniform surface, and has no impurity phase after doping. The doped Ni and S atoms respectively replace the Sn and O atoms in the SnO₂ crystal, decreasing the band gap to 0.014 eV. The oxygen evolution potential of (Ni, S)-SnO₂ reaches the maximum of 1.74 V, the current density reaches maximum and the charge transfer resistance is the lowest, indicating that the electrochemical performance of (Ni, S)-SnO₂ is the best. This study offers an important guide for modification by co-doping to improve the electrochemical performance of SnO₂.

Keywords: (Ni, S)-SnO₂; Hydrothermal method; Co-doping; First principle calculation; Electrochemical performance.

1. INTRODUCTION

Nano SnO₂, as a rutile structure semiconductor material with wide band gap of 3.6 eV[1,2], has many advantages, such as high theoretical capacity of 782 mAh/g, high density capacity, clean and environmental protection, low cost, excellent cycling performance and excellent compactness performance[3-5]. Its actual capacity is much higher than that of carbon negative electrode materials of lithium battery. Therefore, SnO₂ nanomaterials are widely used in various solar cell materials and

excellent semiconductor materials[6,7].

However, SnO₂ has poor conductivity due to its loose internal structure, low density, wide band gap and other defects[8], which limit its application. As such, the structure, morphology and size of SnO₂ are adjusted to improve the electrochemical properties of SnO₂ electrode materials. The morphology and size of nanocrystals can be changed by doping other ions into nanostructures[9]. Moreover, doped ions can create lattice defects and improve band gap, thus improving the electrochemical properties of the materials[10].

According to the different types of doped elements, doping can be divided into non-metallic and metallic doping[11,12]. Although single-element doping can improve the electrocatalytic efficiency of SnO₂ to a certain extent, this effect is not ideal. The repulsive effect of single-element doping results in the non-obvious improvement of SnO₂ electrochemical performance. Yamamoto[13] first proposed that doping two or more elements could effectively improve their crystallinity, crystal structure and band gap. Subsequently, a large number of studies have been reported on two or more elements doping. Indium–gallium (In–Ga) co-doped SnO₂ thin films were prepared by spray pyrolysis[14]. The theoretical and experimental results showed that the hall mobility of (In–Ga) co-doped SnO₂ is three to four orders higher than that of SnO₂:In and SnO₂:Ga. Chen et al.[15] found that F-Sb co-doped SnO₂ electrode has a good electrocatalytic performance on the degradation of methyl orange. In our previous work, we showed that co-doping can improve the photoelectrocatalytic performance of pure SnO₂[16,17].

In this work, we prepared pure SnO₂, Ni-SnO₂, S-SnO₂ and (Ni, S)-SnO₂ nanoparticles by hydrothermal method. Then, the corresponding electrode was prepared by drop coating method. Electrochemical performance tests show that doping can effectively improve the electrochemical performance of SnO₂. Moreover, the electronic structures of the samples were investigated to further illustrate the effect of Ni and S dopants on the electrochemical performance of SnO₂. This study serve as an important guide for modification by co-doping to improve the electrochemical performance of SnO₂.

2. EXPERIMENTAL AND CALCULATIONAL METHODS

2.1 Experimental methods

Pure SnO₂, Ni-SnO₂, S-SnO₂ and (Ni, S)-SnO₂ nanoparticles were prepared by hydrothermal method. Exactly 9.0260g SnCl₂·2H₂O were dissolved in deionised water, and 0.7987g of NiCl₂·6H₂O and 0.8602g of thiocarbazon (n_s: n_{Ni}=1:1) was added to the solution. Then, the solution was transferred to a reaction kettle with polytetrafluoroethylene. After heating at 180 °C for 4 hours, centrifugation and drying, the (Ni, S)-SnO₂ nanoparticles were prepared by high temperature calcining at 350 °C. NiCl₂·6H₂O and thiocarbazon were respectively used as dopants to prepare Ni-SnO₂ and S-SnO₂ nanoparticles. The SnO₂ nanoparticles were prepared without any dopants.

Conductive glass (FTO) with 1 cm × 2 cm size were pre-treated. Hydrochloric acid, anhydrous ethanol and deionised water were used successively for ultrasonic washing, and the samples were dried for use. Then, 0.01 g of the prepared sample powder was added in 1.0 mL of water, and one to two drops

of glycerol were added into the solution. Then, the solution was coated evenly on the pre-treated FTO surface to form a small square of 1 cm × 1 cm. Finally, it was placed in a drying box for use.

The crystal structures of the samples were measured using a D/max-2500 diffractometer with Cu-K α radiation in the 2 θ range from 10° to 85°. Scanning electron microscopy (SEM) images were acquired at an acceleration voltage of 10 kV with a JEOL JEM-2100 instrument. X-ray photoelectron spectroscopy (XPS, AXIS ultra DLD, England) was used to determine the element's valence state.

Electrochemical workstation with 1.0mol/LNa₂SO₄ electrolyte was used to test the electrochemical performance, such as the cyclic voltammetric curves (CV), linear sweep voltammetric curve (LSV) and electrochemical impedance curve (EIS). The prepared electrode, Pt electrode and the calomel electrode were respectively used as working electrode, auxiliary electrode and reference electrode. The frequency range of EIS was 10⁻²-10⁵ Hz, and the scan rate was 0.05 V/s. The conductivity value was calculated according to the following formula:

$$\sigma = \frac{4d}{R\pi D^2} \quad 1-1$$

In this formula, σ represents the conductivity value, S/cm. d represents the average thickness, cm. R represents the impedance values in impedance spectrum, Ω . D represents the electrode diameter, cm.

2.2 Computational methods

The electronic structure of SnO₂ was calculated by Castep software[18] based on density functional theory. Perdew-Burke-Ernzerh(PBE) functional of General Gradient Approximation (GGA) was used to describe the exchange correlation potential[19]. The cutoff energy of plane wave was set as 340 eV, and the 4×4×3 Monkhorst-Pack scheme[20] was adopted for the Brillouin zone integrations. The energy convergence accuracy was 2.0×10⁻⁵ eV/atom, the convergence standard of interatomic interaction was 0.03 eV/Å, and the maximum stress was 0.1 GPa.

In the calculation process, a 2×2×2 SnO₂ supercell with 48 atoms was used as the calculation model. For Ni-SnO₂, S-SnO₂ and (Ni, S)-SnO₂ models, metal atom Ni replaced Sn atom in the crystal body center, and the equivalent S atom replaced the coplanar O atom. The optimised lattice parameters of pure SnO₂ were firstly calculated to ensure the reliability of the calculation. The optimized lattice parameters (a=4.737 Å and c=3.186 Å) were consistent with other results (a=4.734 Å, c=3.187 Å)[21].

3. RESULTS AND DISCUSSION

As shown in Figure 1, compared with that of pure SnO₂, the surface distribution of Ni-SnO₂, S-SnO₂ and (Ni, S)-SnO₂ nanoparticles is more uniform, the agglomeration phenomenon is reduced and the particle sizes are smaller. For (Ni, S)-SnO₂, the particle distribution is the most uniform, and the particle is in the shape of a small ball, indicating that it has a large specific surface area, which is conducive to charge transfer.

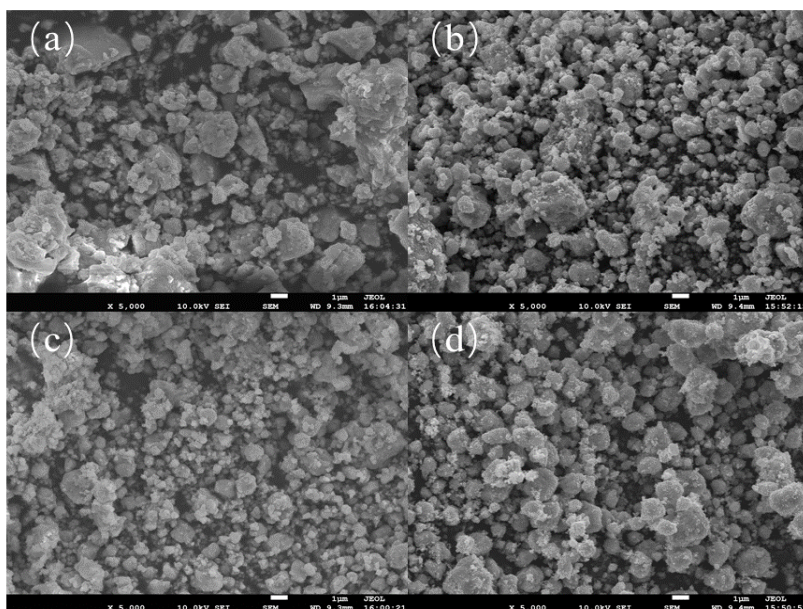


Figure 1. SEM images of pure SnO₂(a), Ni-SnO₂(b), S-SnO₂(c) and (Ni, S)-SnO₂(d) nanoparticles

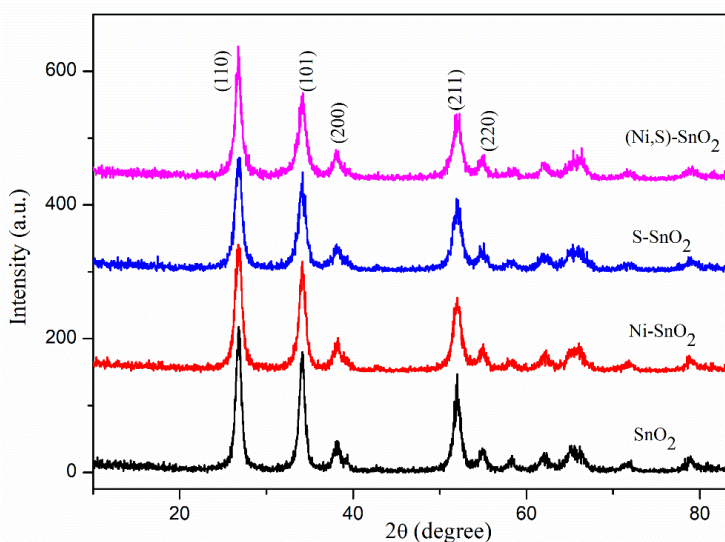


Figure 2. XRD patterns of pure SnO₂, Ni-SnO₂, S-SnO₂ and (Ni, S)-SnO₂ nanoparticles

X-ray diffraction (XRD) analysis was performed before and after doping to investigate the effect of doped elements on the crystal configuration of SnO₂. In Figure 2, the structures of Ni-SnO₂, S-SnO₂ and (Ni, S)-SnO₂ are consistent with the standard rutile structure of SnO₂. At $2\theta=26.506^\circ$, 33.945° and 51.940° , the corresponding crystal planes are respectively (110), (101) and (211)[22]. Given the low dopant level[23] and partial substitution of dopant ions in the SnO₂ lattice sites[24], no diffraction peaks associated with Ni or its oxide appeared, indicating that they are still rutile SnO₂ structures. However, after doping, the diffraction peak strength is slightly weakened, and the half-peak width becomes wider, indicating that the doping of elements into the SnO₂ lattice results in the reduction of the order degree of atoms, inhibiting the growth of grain and leading to the reduction of crystallinity and grain size[25].

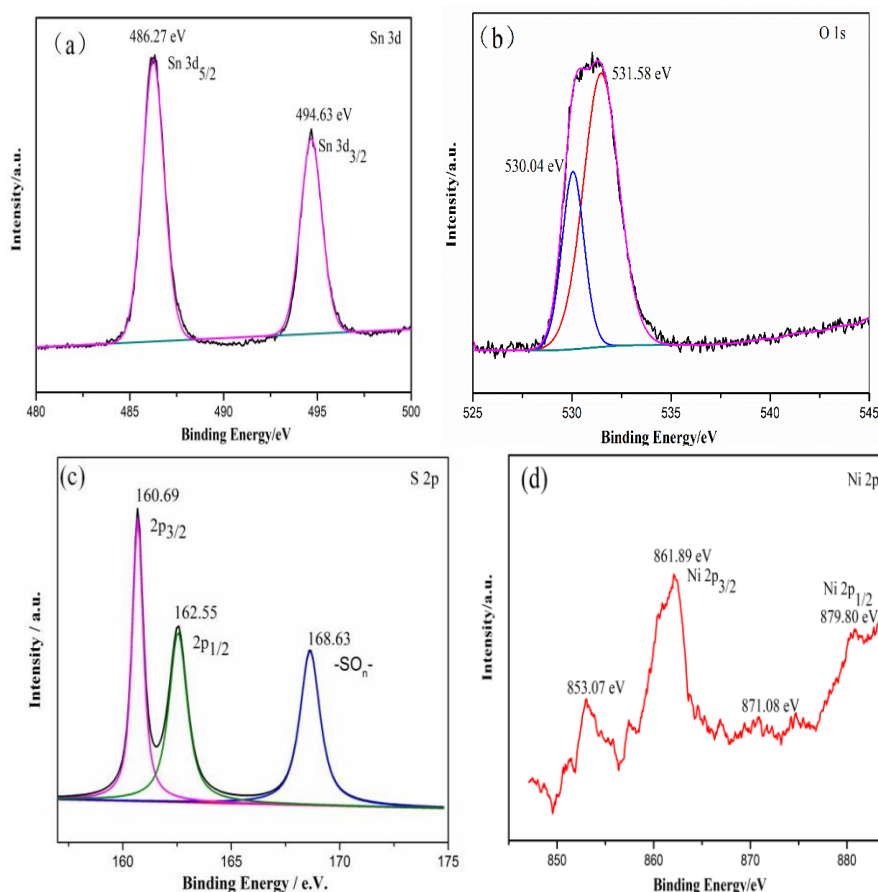


Figure 3. XPS spectra of Sn 3d(a), O 1s(b), S 2p(c) and Ni 2p(d)

The XPS spectra of (Ni, S)-SnO₂ shown in Figure 3 are analysed to determine the chemical composition and elemental valence states of SnO₂ by Ni and S co-doping. Figure 3(a) shows that the high strength peaks at 486.27 and 494.63 eV respectively correspond to Sn 3d_{5/2} and Sn 3d_{3/2}. The difference value of binding energy between the two peaks is 8.36 eV, which is exactly the same as the difference value of binding energy of Sn⁴⁺ ions in SnO₂ crystal[26,27], indicating the presence of SnO₂. The peaks of O 1s can be divided into two types. The peak at 530.04 eV is caused by lattice oxygen in NiO and SnO₂, indicating the formation of metal oxides. The peak at 531.58 eV is related to the adsorption oxygen of the surface[28]. For S 2p, there existed three peaks, the peaks at 160.69 eV and 162.55 eV can be assigned to S 2p_{3/2} and S 2p_{1/2}, suggesting the presence of S²⁻. The peak at 168.63 eV indicates the existence of S⁶⁺, which may be due to the adsorption of SO₄²⁻ on the surface[29]. Figure 3(d) showed the XPS spectra of Ni 2p. The main peak at 853.07 eV and satellite peak at 853.07 eV can be assigned to Ni 2p_{3/2}, and the peaks at 871.08 eV and 879.80 eV can be distributed to Ni 2p_{1/2}, suggesting the presence of Ni²⁺[30].

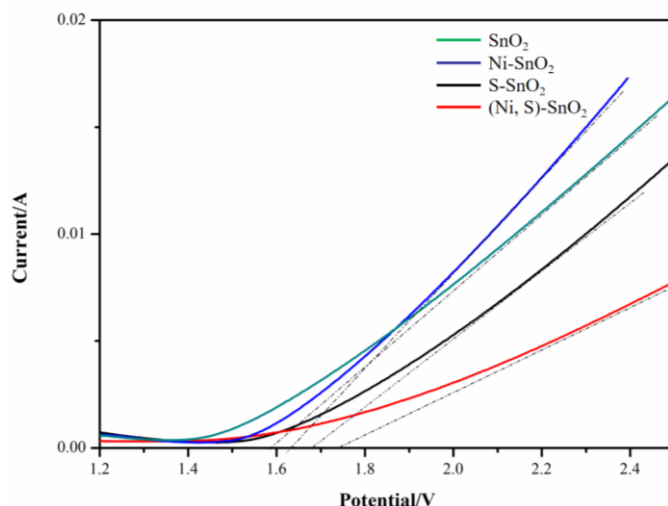


Figure 4. LSV curves of pure SnO_2 (a), Ni-SnO_2 (b), S-SnO_2 (c) and $(\text{Ni, S})\text{-SnO}_2$ (d) electrodes with a scan rate of 0.05 V/s

LSV curve can indirectly reflect the electrochemical activity of the electrode, and the value of oxygen evolution potential can represent the difficulty level of oxygen evolution side reaction. The larger the oxygen evolution potential, the higher the electrocatalytic activity of the electrode. Figure 4 shows the LSV curves of pure SnO_2 , Ni-SnO_2 , S-SnO_2 and $(\text{Ni, S})\text{-SnO}_2$ electrodes.

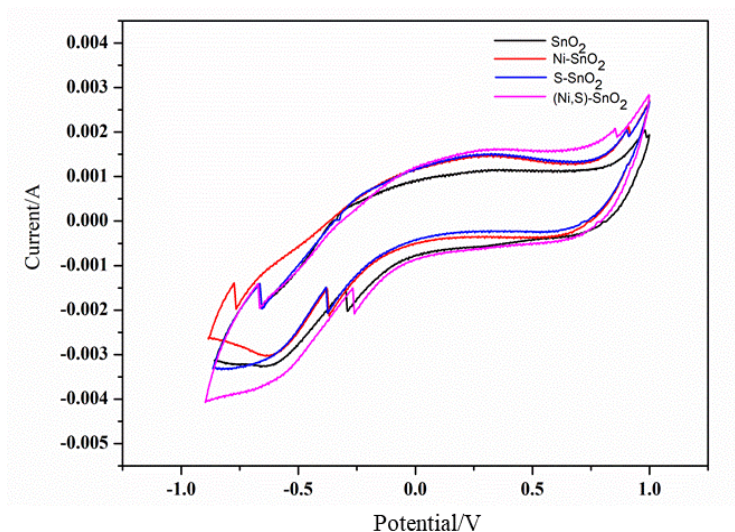


Figure 5. CV curves of pure SnO_2 (a), Ni-SnO_2 (b), S-SnO_2 (c) and $(\text{Ni, S})\text{-SnO}_2$ (d) electrodes with a scan rate of 0.05 V/s

The intersection point of the tangent line of the current curve and the abscissa is the oxygen evolution potential. The oxygen evolution potentials of pure SnO_2 , Ni-SnO_2 , S-SnO_2 and $(\text{Ni, S})\text{-SnO}_2$ electrodes are respectively 1.59, 1.63, 1.69 and 1.74 V. Compared with pure SnO_2 , all of the oxygen

evolution potentials increased after doping. After Ni and S co-doping, the oxygen evolution potential increased to 1.74 V, indicating that co-doping can increase the oxygen evolution potential of electrodes, reduce the occurrence of oxygen evolution side reaction and improve the electrocatalytic performance of electrodes. Pure SnO₂ is prone to forming oxygen vacancies on its surface, which can generate oxygen vacancy effect and result in high resistivity[31]. Doping can reduce the electron-hole recombination, narrow the band gap, reduce its resistivity and improve the oxygen evolution potential. For (Ni, S)-SnO₂ electrodes, the oxygen evolution potential reached the maximum, and the electrocatalytic performance of the electrode is the best.

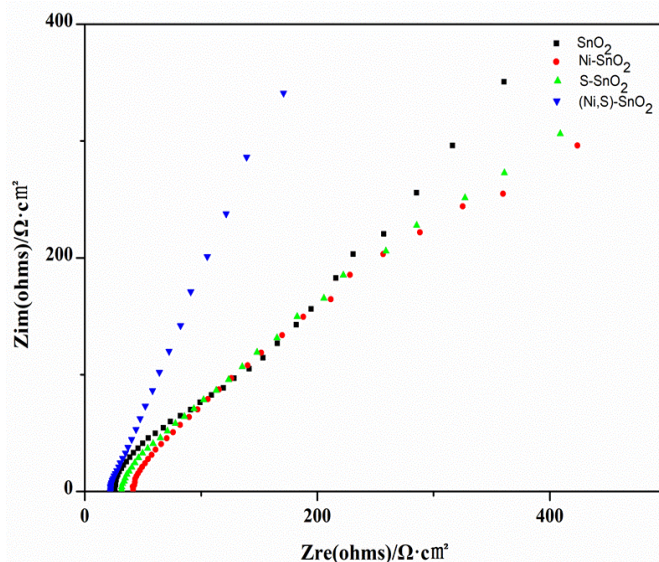


Figure 6. EIS curves of pure SnO₂(a), Ni-SnO₂(b), S-SnO₂(c) and (Ni, S)-SnO₂(d) electrodes at 0.5 V bias voltage

Table 1. Electrical conductivity values of pure SnO₂, Ni-SnO₂, S-SnO₂ and (Ni, S)-SnO₂ electrodes

	electrical conductivity value(S/cm)
SnO ₂	1.45×10^{-3}
Ni-SnO ₂	2.55×10^{-3}
S-SnO ₂	4.25×10^{-3}
(Ni, S)-SnO ₂	7.08×10^{-3}
Sm-CeO ₂	3.3×10^{-3} [32]
Y-CeO ₂	3.4×10^{-3} [33]
Zn _{0.1} Sn _{0.9} P ₂ O _{7-δ}	2.84×10^{-6} [34]
MnO ₂ /PAN	2.82×10^{-3} [35]
10SnO ₂ ·10P ₂ O ₅ ·10Fe ₂ O ₃ ·70V ₂ O ₅	4.6×10^{-5} [36]

The CV curves of SnO₂, Ni-SnO₂, S-SnO₂ and (Ni, S)-SnO₂ electrodes were tested to further investigate the activity of the electrodes. Figure 5 shows that the CV curves are roughly symmetrical,

suggesting that the conversion process of doping electrode surfaces is reversible. The response current density changes obviously after doping. For (Ni, S)-SnO₂ electrodes, the current density increases the most. This result may be caused by the Ni and S co-doping into the SnO₂ lattice, which increases the crystal surface area and further improves the electrocatalytic activity of the electrode.

Figure 6 shows the EIS spectra of electrodes with different doping conditions. The curve shape of each sample is the same. The high frequency area shows a semicircle shape and the diameter of the semicircle represents the charge transfer resistance. For the low frequency area, the line represents the diffusion resistance, and the closer the line to 90°, the smaller the diffusion resistance. Compared with that of pure SnO₂, the charge transfer resistance of Ni-SnO₂, S-SnO₂ and (Ni, S)-SnO₂ decrease. The corresponding electrical conductivity values are listed in Table 1. The electrical conductivity values of pure SnO₂, Ni-SnO₂, S-SnO₂ and (Ni, S)-SnO₂ electrodes are 0.00145, 0.00255, 0.00425 and 0.00708 S/cm, respectively. The co-doping of Ni and S elements makes the charge transfer resistance reach the minimum, indicating that co-doping can improve the electrochemical performance of SnO₂. Meanwhile, compared with other doped conductive materials, (Ni, S)-SnO₂ shows excellent electrochemical performance.

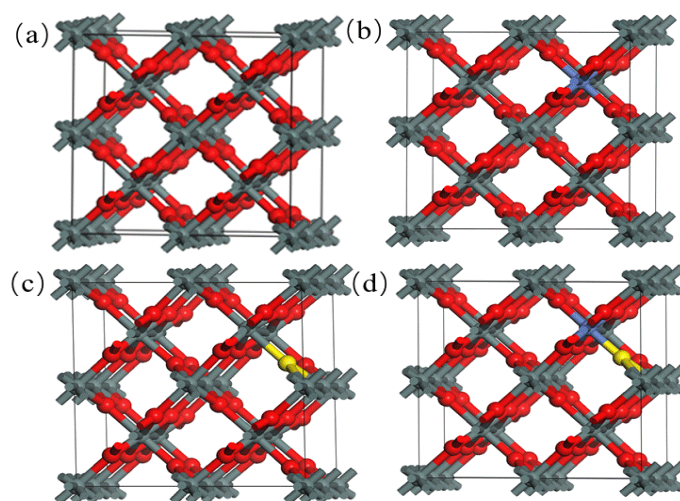


Figure 7. 2×2×1 crystal structures of pure SnO₂(a), Ni-SnO₂(b), S-SnO₂(c) and (Ni, S)-SnO₂(d)

Table 2. Lattice parameters of 2×2×1 SnO₂, Ni-SnO₂, S-SnO₂ and (Ni, S)-SnO₂ supercells

	a=b(Å)	c(Å)
SnO ₂	9.475	6.373
Ni-SnO ₂	9.795	6.524
S-SnO ₂	9.934	6.588
(Ni,S)-SnO ₂	9.873	6.549

The electronic structures of SnO₂, Ni-SnO₂, S-SnO₂ and (Ni, S)-SnO₂ were investigated using first-principles calculations to illustrate the effect of Ni and S dopants on the electrochemical performance of SnO₂. The optimised structures are shown in Figure 7.

As shown in Table 2, the lattice parameters of 2×2×1 SnO₂ are a=b=9.475 Å and c=6.373 Å. Considering the different ions radii between dopants and host lattice atoms, doped ions will change the crystal structure of different doping models. For Ni-SnO₂, the lattice parameters change to a=b=9.795 Å and c=6.524 Å, and this result can be attributed to the radius of Ni²⁺ ion that is greater than that of Sn⁴⁺ (Ni²⁺:0.72 Å, Sn⁴⁺:0.71 Å). Similarly, given that the radius of S²⁻ ion is larger than that of O²⁻ ion (S²⁻:1.84 Å, O²⁻:1.40 Å), the lattice parameters a and c of S-SnO₂ increase. When S and Ni are co-doped, the lattice parameters are a=b=9.873 Å and c=6.549 Å, respectively.

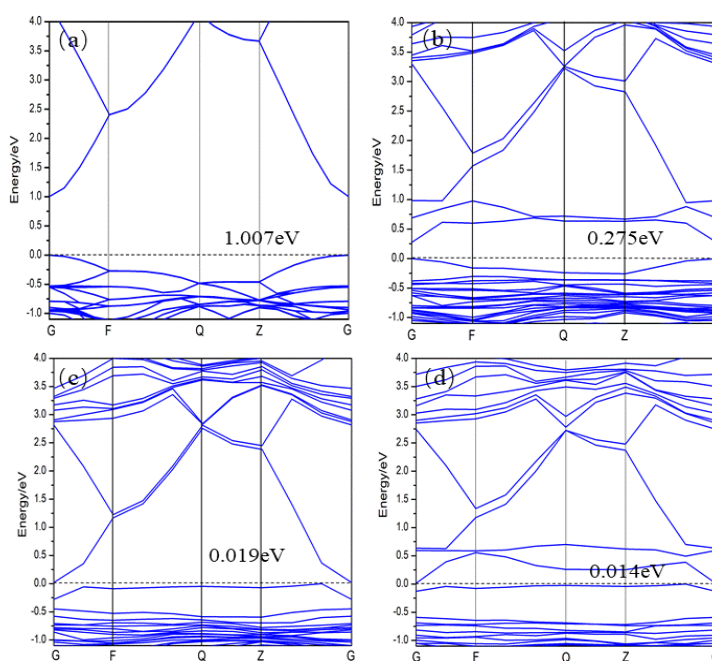


Figure 8. Band gaps of pure SnO₂(a), Ni-SnO₂(b), S-SnO₂(c) and (Ni, S)-SnO₂(d)

Introducing doped ions will not only change its configuration, but will also affect its electronic structure. Furthermore, the electrochemical properties are affected.

The band gap of SnO₂ (Figure 8) is 1.007 eV, which is consistent with other theoretical calculation[31]. However, the band gap value is lower than the actual band gap value of 3.6 eV, which is due to the underestimation of the LDA function to association energy. Besides, the strong Coulomb correlation between electrons is not well described. Here, the underestimation does not affect the theoretical analysis of electronic structure. After doping, the band gaps become denser, interband fluctuations become more gradual and all of the band gaps decrease obviously. For Ni-SnO₂, the position of the conduction band moves down, which makes the band gap narrow to 0.275 eV. For S-SnO₂ and (Ni, S)-SnO₂, the band gaps are respectively 0.019 eV and 0.014 eV.

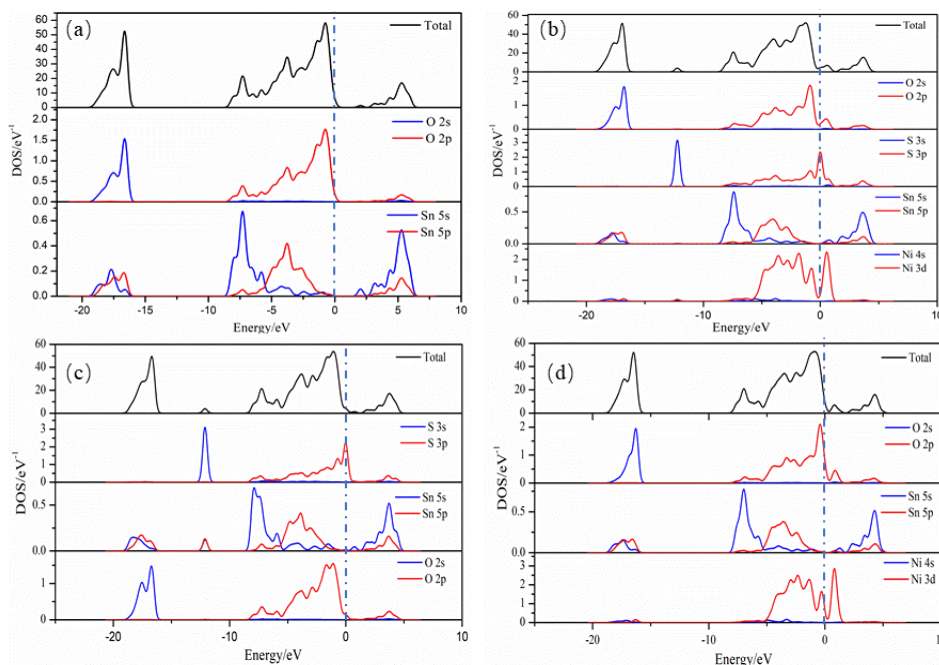


Figure 9. DOS of pure SnO₂(a), Ni-SnO₂(b), S-SnO₂(c) and (Ni, S)-SnO₂(d)

Figure 9 shows that the doping of Ni and S atoms into the rutile SnO₂ lattice causes shifts of the valence and conduction band edges and the introduction of impurity states in the band gap. The Sn 5s and 5p states contribute to the conduction band and the O 2p states mainly contribute the valence band. After Ni doping, the bottom of the conduction band mainly consists of Ni 3d states. The top of the valence band mainly consists of O 2p states, as well as a small contribution from the Ni 3d states. When S is doped alone into the SnO₂ lattice, a new impurity peak is formed at -12.5 eV, which widens the valence band and is made up of S 3s states, mixing a few Sn 5p states. At the Fermi level, the DOS at the top of the valence band is supplied by S 3p states instead of O 2p states, which narrows the band gap to 0.275 eV. In the Ni and S co-doped system, new energy levels are introduced at the top of the valence band, and the new energy level forms the top of the valence band. Given that the 3p state energy level of S is higher than that of O 2p, it can provide more holes and the valence band will move up. For the bottom of the conduction band, the hybridisation of S 3p, Sn 5s and Ni 3d states decreases the width of conduction band. Thus, the degree of electron co-ownership is increased, the local property is enhanced, and the conductivity is improved compared with that of single doping.

4. CONCLUSION

Pure SnO₂, Ni-SnO₂, S-SnO₂ and (Ni,S)-SnO₂ nanoparticles were prepared by hydrothermal method to improve the electrochemical performance of SnO₂. After doping, the crystal structure retained rutile SnO₂ with homogeneous surface. The Ni and S atoms were co-doped into SnO₂ crystal with valence states of Ni²⁺ and S²⁻. The electrochemical performance test showed that the oxygen evolution potential of (Ni,S)-SnO₂ increased to 1.74 V, the current density reached the maximum, and the charge

transfer resistance was the lowest, indicating (Ni,S)-SnO₂ had the best electrochemical performance. Otherwise, the band gap decreased from 1.007 eV to 0.014 eV after Ni and S co-doping, which are conducive to the electrochemical performance. Hence, (Ni,S)-SnO₂ can be an ideal alternative anode material for electrochemistry.

ACKNOWLEDGEMENTS

This work is funded by Science and Technology Innovation Project of Colleges and Universities in Shanxi Province (No.2019L0842) and "Shanxi 1331 project" key discipline construction plan (2017, 122)

References

1. S. Das, V. Jayaraman, *Prog. Mater. Sci.*, 66 (2014) 112.
2. C. Drake, S. Seal, *Appl. Phys. Lett.*, 90 (2007) 233117.
3. R.B. Dupraz, C. Johansen, K. Dupraz, T. Jaouen, P. Aebi, U. Steiner and A. Abate, *J. Mater. Chem. A*, 6 (2018) 1850.
4. W. Chen, Y.C. Qiu, S.H. Yang, *Phys. Chem. Chem. Phys.*, 12 (2010) 9494.
5. H.J. Snaith, C. Ducati, *Nano Lett.*, 10 (2010) 1259.
6. Z.Z. Liu, K.M. Deng, J. Hu and L. Li, *Angew. Chem. Int. Edit.*, 58 (2019) 11497.
7. I. Bedja, P.V. Kamat, *J. Phys. Chem.*, 99 (1995) 9182.
8. S. Das, V. Jayaraman, *Prog. Mater. Sci.*, 66 (2014) 112.
9. S.X. Yu, L.W. Yang, Y.C. Li, X. Qi, X.L. Wei and J.X. Zhong, *J. Cryst. Growth*, 367 (2013) 62.
10. K. Ueda, H. Tabata, T. Kawai, *Appl. Phys. Lett.*, 79 (2001) 988.
11. K. Xu, S.Q. Tian, J. Zhu, Y. Yang, J. Shi, T. Yua and C.L. Yuan, *Nanoscale*, 10 (2018) 20761.
12. J.W. Liang, Z.L. Chen, G. Yang, H.B. Wang, F.H. Ye, C. Tao and G.J. Fang, *ACS Appl. Mater. Interfaces*, 11 (2019) 23152.
13. T. Yamamoto, H. Katayama-Yoshida, *Jpn. J. Appl. Phys. pt Lett.*, 38 (1999) 166.
14. Q.N. Mao, Z.G. Ji, L.N. Zhao, *Phys. Status Solidi B*, 247 (2010) 299.
15. L.S. Chen, Y.Y. Liu, H.X. Li, C. Liu and K. Wu, *Adv. Mater. Res.*, 465 (2012) 192.
16. M.M. Guo, H.M. Yang, E.H. Zhang, M.T. Gao, Z.H. Liang and P. D. Han, *J. Alloy. Compd.*, 742 (2018) 721.
17. M.M. Guo, H.M. Yang, M.T. Gao, E.H. Zhang, Z.H. Liang and P. D. Han, *Rsc Adv.*, 7 (2017) 42940.
18. V. Milman, K. Refson, S.J. Clark, C.J. Pickard, J.R. Yates, S.P. Gao, P.J. Hasnip, M.I.J. Probert, A. Perlov and M.D. Segall, *J. Mol. Struct. THEOCHEM*, 954 (2010) 22.
19. Z. Szekeres, F. Bogár, J. Ladik, *Int. J. Quantum Chem.*, 102 (2005) 422.
20. H.J. Monkhorst, J.D. Pack., *Phys. Rev. B*, 16 (1976) 1748.
21. B. Thangaraju, *Thin Solid Films*, 402 (2002) 71.
22. F.A. Akgul, C. Gumus, A.O. Er, A.H. Farha, G. Akgul, Y. Ufuktepe and Z. Liu, *J. Alloy. Compd.*, 579 (2013) 50.
23. Y.H. Cui, Y.J. Feng, Z.Q. Liu, *Electrochim. Acta*, 54 (2009) 4903.
24. A.R. Babar, S.S. Shinde, A.V. Moholkar, C.H. Bhosale, J.H. Kim and K.Y. Rajpure, *J. Alloy. Compd.*, 505 (2010) 416.
25. Y. Sun, S.A. Cheng, Z. Yu, L.X. Li, C.C. Li and J.W. Yang, *J. Alloy. Compd.*, 834 (2020) 155184.
26. I. Ullah, A. Munir, S. Muhammad, S. Ali, N. Khali, M. Zubair, M. Sirajuddin, S.Z. Hussain, S. Ahmed, Y. Khan, I. Hussain and A. Haider, *J. Alloy. and Compd.*, 827 (2020) 154247.

27. B. Babu, I.N. Reddy, K. Yoo, D. Kim and J. Shim, *Mater. Lett.*, 221 (2018) 211.
28. I.M. Costa, Y.N. Colmenares, P.S. Pizani, E.R. Leite and A.J. Chiquito, *Chem. Phys. Lett.*, 695 (2018) 125.
29. J.O. Olowoyo, M. Kumar, S.L. Jain, S.H. Shen, Z.H. Zhou, S.S. Mao, A.V. Vorontsov and U. Kumara, *Int. J. Hydrogen Energy*, 43 (2018) 17682.
30. W. Dai, X. Pan, S.S. Chen, C. Chen, Z. Wen, H.H. Zhang and Z.Z. Ye, *J. Mater. Chem. C*, 2 (2014) 4606.
31. K. Bakht, T. Mahmood, M. Ahmed and K. Abid, *Superlattice. Microst.*, 90 (2016) 236.
32. A. Pappacena, P. Porreca, M. Boaro, C. Leitenburg and A. Trovarelli, *Int. J. Hydrogen Energy*, 37 (2012) 1698.
33. A.J. Jacobson, *Chem. Mater.*, 22 (2009) 660.
34. S.R. Phadke, C.R. Bowers, E.D. Wachsman and J.C. Nino, *Solid State Ionics*, 183 (2011) 26.
35. D.R. Chang, G.S. Heo, *e-Polymers*, 11 (2011) 1.
36. K. Mastsuda, S. Kubuki, K. Akiyama, Z. Homonnay, K. Sinko, E. Kuzmann and T. Nishida, *J. Cera. Soc. Jpn.*, 123 (2015) 121.

© 2021 The Authors. Published by ESG (www.electrochemsci.org). This article is an open access article distributed under the terms and conditions of the Creative Commons Attribution license (<http://creativecommons.org/licenses/by/4.0/>).